An edge-preserving multilevel method for deblurring, denoising, and segmentation

S. Morigi[1], L. Reichel[2], and F. Sgallari[1]

[1] Dept. of Mathematics-CIRAM, University of Bologna, Bologna, Italy
{morigi,sgallari}@dm.unibo.it
[2] Dept. of Mathematical Sciences, Kent State University, Kent, OH 44242, USA
reichel@math.kent.edu

Abstract. We present a fast edge-preserving cascadic multilevel image restoration method for reducing blur and noise in contaminated images. The method also can be applied to segmentation. Our multilevel method blends linear algebra and partial differential equation techniques. Regularization is achieved by truncated iteration on each level. Prolongation is carried out by nonlinear edge-preserving and noise-reducing operators. A thresholding updating technique is shown to reduce "ringing" artifacts. Our algorithm combines deblurring, denoising, and segmentation within a single framework.

1 Introduction

Digital image restoration, reconstruction, and segmentation are important in medical and astronomical imaging, film restoration, as well as in image and video coding. This paper introduces a cascadic multilevel method for simultaneous restoration and segmentation of blurred and noisy images. Blur arises for many reasons, including out-of-focus cameras, and camera or object motion during exposure. Blur often is modeled by a point-spread function (PSF). Noise is the random, unwanted, variation in brightness of an image. It may originate from, e.g., film grain or electronic noise from a digital camera or scanner. We consider additive noise in this work.

It is well known that linear deblurring methods tend to introduce oscillatory artifacts. Variational deblurring methods are able to reduce these artifacts, however, they typically are much more computationally intensive than linear methods; see, e.g., Welk et al. [15] for a discussion.

Many segmentation methods apply curve evolution techniques. These methods seek to detect object boundaries, represented by closed curves in an image. The contours are represented as the zero level set of an implicit function defined in higher dimension. The active contours evolve in time according to a PDE model, which takes into account intrinsic geometric measures of the image. We will use a variant proposed by Li et al. [7] of the well-known Geodesic Active Contours (GAC) model [2].

This paper discusses a cascadic multilevel image restoration method that allows both spatially variant and spatially invariant PSFs. The method requires

the solution of a linear system of equations on each level. These systems are solved by an iterative method, the choice of which depends on properties of the PSF. We introduce a thresholding updating strategy in order to suppress "ringing." The restriction operators are defined by solving local weighted least-squares problems, and the prolongation operators are determined by piecewise linear prolongation followed by integrating a discretized nonlinear Perona-Malik diffusion equation for a few time-steps. The purpose of the integration is to reduce noise. The cascadic multilevel method so obtained shares the computational efficiency and simplicity of truncated iteration for the solution of linear discrete ill-posed problems with the edge-preserving property of nonlinear models. The multilevel method proceeds from coarser to finer levels, and regularizes by truncated iteration on each level. For many image restoration problems, the multilevel method demands fewer matrix-vector product evaluations on the finest level than the corresponding 1-level truncated iterative method, and often determines restorations of higher quality. A benefit of our multilevel approach to image restoration is that it easily can be combined with image segmentation, as is illustrated in the present paper. We remark that our multilevel method differs significantly from multilevel methods for the solution of well-posed boundary value problems for elliptic partial differential equations in that prolongation and restriction operators, as well as the number of iterations on each level are chosen in a different manner.

This paper is organized as follows. Section 2 introduces the variational deblurring and the denoising model, Section 3 discusses the cascadic multilevel framework, and Section 4 presents a few computed examples. Concluding remarks can be found in Section 5.

2 Deblurring, denoising, and segmentation of images

We consider the restoration of two-dimensional gray-scale images, which have been contaminated by blur and noise. The available observed blur- and noise-contaminated image f^δ is related to the unavailable blur- and noise-free image $\hat{u}$ by the degradation model

$$f^\delta(x) = \int_\Omega h(x,y)\hat{u}(y)dy + \eta^\delta(x), \qquad x \in \Omega, \tag{1}$$

where $\Omega \subset \mathbb{R}^2$ is the image domain, η^δ represents noise in the data, and the kernel $h(x,y)$ models the PSF. If the blur is spatially invariant, then h is of the form $h(x,y) = \tilde{h}(x-y)$ for some function $\tilde{h}$. The kernel is smooth or piecewise smooth and, therefore, the integral operator is compact. It follows that the solution of (1) is an ill-posed problem; see, e.g., Engl et al. [3] and Hansen [5] for discussions on ill-posed problems and their numerical solution.

We would like to determine an accurate approximation of $\hat{u}$ when the observed image f^δ and the kernel h, but not the noise η^δ, are known. A popular

approach to achieving this is to minimize the functional

$$E(u) = \int_\Omega \frac{1}{2} \left(\int_\Omega h(x,y)u(y)dy - f^\delta(x) \right)^2 + \rho\, R(u(x))dx, \tag{2}$$

where $\rho > 0$ is a regularization parameter and

$$R(u) = \psi(|\nabla u|^2) \tag{3}$$

is a regularization operator. Here ψ is a differentiable monotonically increasing function and ∇u denotes the gradient of u; see, e.g., Rudin et al. [11] and Welk et al. [15] for discussions on this kind of regularization operators.

The Euler-Lagrange equation associated with (2), supplied with a gradient descent which yields a minimizer as "time" $t \to \infty$, is given by

$$\frac{\partial u}{\partial t}(t,z) = -\int_\Omega h(x,z) \left(\int_\Omega h(x,y)u(t,y)dy - f^\delta(x) \right) dx + \rho\, D(u(t,z)), \tag{4}$$

for $z \in \Omega$ and $t \geq 0$. The initial function $u(0,z) = f^\delta(z)$, $z \in \Omega$, and suitable boundary conditions are used. We also refer to D as a regularization operator. Image restoration methods based on the Euler-Lagrange equation require that the regularization operator D, as well as values of the regularization parameter ρ and a suitable finite time-interval of integration $[0,T]$ be chosen. The determination of suitable values of ρ and T generally is not straightforward.

We get from (3) that

$$D(u) = \mathrm{div}(g(|\nabla u|^2)\nabla u), \qquad g(t) = d\Psi(t)/dt. \tag{5}$$

The function g is referred to as the diffusivity. Perona-Malik regularization is obtained by choosing the diffusivity

$$g(s) = \frac{1}{1 + s/\sigma}, \tag{6}$$

where σ is a positive constant; see [14]. Alternatively, one can use a regularization operator of total variation-type.

Nonlinear models based on (4)-(6) can provide denoising and deblurring of good quality; however, their time-integration is computationally demanding: explicit methods require many tiny time-steps and therefore are expensive, while each time-step with an implicit or semi-implicit method is, in general, expensive even if it could be accelerated by multigrid techniques.

A much cheaper and simpler approach to determining an approximation of the desired image $\hat{u}$ is to apply a few steps of an iterative method to the linear system of equations obtained by a discrete approximation of (1),

$$Au = b^\delta, \qquad A \in \mathbb{R}^{n\times n}, \qquad u, b^\delta \in \mathbb{R}^n. \tag{7}$$

Here A is a discrete blurring operator and b^δ represents the available blur- and noise-contaminated image. In applications typically b^δ, rather than f^δ, is available; see [5] for details.

Approximate solutions of (7) conveniently can be computed by Krylov subspace iterative methods, where the choice of method depends on the matrix properties. For instance, spatially variant blur often gives rise to a nonsymmetric matrix A, and we may use the LSQR Krylov subspace method [13] to solve (7). This method is an implementation of the conjugate gradient method applied to the normal equations. When the matrix is symmetric, but possibly indefinite, the MR-II [4] Krylov subspace method is an attractive alternative to LSQR. The iteration number may be considered a discrete regularization parameter. It is important not to carry out too many iterations in order to avoid severe error propagation. This approach to determining a restored image is referred to as regularization by truncated iteration; see, e.g., [3, 4, 8] for discussions. Due to cut-off of high frequencies, these iterative methods may introduce artifacts, such as ringing, and fail to recover edges accurately.

Many image analysis applications require image segmentation. The level to which segmentation is carried out depends on the problem being solved; segmentation should be terminated when the regions of interest in the application have been isolated. This problem-dependence makes autonomous segmentation one of the most difficult computational tasks in image analysis. The presence of noise and blur makes this task even more complicated. In this paper we carry out segmentation by computing Geodesic Active Contours (GAC). This kind of segmentation methods are based on curve evolution theory, see [2] and references therein, and level sets [12]. The basic idea is to start with initial boundary shapes represented by closed curves, i.e., contours, and iteratively modify these contours by application of shrink/expansion operations determined by image constraints. The shrink/expansion operations, referred to as contour evolution, are performed by minimizing an energy functional, similarly to traditional region-based segmentation methods; however, the level set framework provides more flexibility.

The GAC PDE model proposed in [2] is given by

$$\frac{\partial \phi}{\partial t} = |\nabla \phi| \mathrm{div}\left(g(|\nabla b^{\delta}|^2) \frac{\nabla \phi}{|\nabla \phi|} \right), \tag{8}$$

where the edge-detector function g is defined by (6) and the initial condition ϕ_0 is the signed distance function to an arbitrary initial curve enclosing the objects to be segmented. The solution to the segmentation problem is the zero-level set of the steady state of the flow $\phi_t = 0$. We apply a fast curve evolution method recently suggested by Li et al. [7] in our multilevel method, which eliminates the need of costly re-initialization, but remark that other GAC methods also can be used.

3 The cascadic multilevel framework

We first review the cascadic multilevel method proposed in [8] for the removal of blur and noise. In [8] only symmetric blurring matrices are considered. Introduce

for $v = [v^{(1)}, v^{(2)}, \ldots, v^{(n)}]^T \in \mathbb{R}^n$ the weighted least-squares norm

$$\|v\| = \left(\frac{1}{n} \sum_{i=1}^{n} \left(v^{(i)} \right)^2 \right)^{1/2}. \tag{9}$$

Let $\hat{b} \in \mathbb{R}^n$ denote the unknown noise-free right-hand side associated with the right-hand side b^δ of (7). We assume that $\hat{b} \in \text{Range}(A)$ and that a bound δ for the noise $e = b^\delta - \hat{b}$ is available, i.e.,

$$\|e\| \leq \delta. \tag{10}$$

Let $W_1 \subset W_2 \subset \cdots \subset W_\ell$ be a sequence of nested subspaces of $\mathbb{R}^n$ of dimension $\dim(W_i) = n_i$ with $n_1 < n_2 < \ldots < n_\ell = n$. We refer to the subspaces W_i as levels, with W_1 being the coarsest and $W_\ell = \mathbb{R}^n$ the finest level. Each level is furnished with a weighted least-squares norm; level W_i has a norm of the form (9) with n replaced by n_i. We choose $n_{i-1} = n_i/4$, $1 < i \leq \ell$.

Let $A_i \in \mathbb{R}^{n_i \times n_i}$ be the representation of the blurring operator A on level W_i. The matrix A_i is determined by discretization of the integral operator (1) similarly as A. This defines implicitly the restriction operator $R_i : \mathbb{R}^n \to W_i$, such that

$$A_i = R_i A R_i^*. \tag{11}$$

We define $R_\ell = I$.

The choice of restriction operators R_i is in our experience less crucial for achieving high-quality restorations than the choice of restriction operators $R_i^{(\omega)} : \mathbb{R}^n \to W_i$ for reducing the available blur- and noise-contaminated image represented by the right-hand side b^δ in (7). We let

$$b_i^\delta = R_i^{(\omega)} b^\delta, \qquad 1 \leq i < \ell, \tag{12}$$

where the $R_i^{(\omega)}$ are determined by repeated local weighted least-squares approximation, inspired by a "staircasing"-reducing scheme recently proposed by Buades et al. [1].

Also the choice of prolongation operators from level $i-1$ to level i is important for the performance of the multilevel method. We apply nonlinear prolongation operators $P_i : W_{i-1} \to W_i$, $1 < i \leq \ell$, defined by piecewise linear interpolation followed by integration of the Perona-Malik equation over a short time-interval; see below. The P_i are designed to be noise-reducing and edge-preserving.

The multilevel methods of the present paper are cascadic, i.e., they first determine an approximate solution of $A_1 u = b_1^\delta$ in W_1, using the LSQR or MR-II iterative methods. We refer to the iterative method as IM in Algorithm 1 below. The iterations with this method are terminated by the discrepancy principle; see below. The so determined approximate solution in W_1 is mapped into W_2 by the prolongation P_2. A correction of this mapped iterate in W_2 is computed by the IM. Again, the iterations are terminated by the discrepancy principle, and the approximate solution in W_2 so obtained is mapped into W_3

Multilevel Algorithm 1

Input: A, b^δ, δ, $\ell \geq 1$ (number of levels);
Output: approximate solution $u_\ell \in W_\ell$ of (7); segmented result ϕ_ℓ;
Determine A_i and b_i^δ from (11) and (12), respectively, $1 \leq i \leq \ell$;
$u_0 := 0$; $\phi_0 :=$ initial contour;
for $i := 1, 2, \ldots, \ell$ do
$u_{i,0} := P_i u_{i-1}$; $\phi_{i,0} := S_i \phi_{i-1}$;
$\Delta u_{i,m_i} := \mathrm{IM}(A_i, b_i^\delta - A_i u_{i,0})$;
Correction step: $u_i := u_{i,0} + \beta \Delta u_{i,m_i}$;
Segmentation step: $\phi_i := GAC(\phi_{i,0}, u_i)$;
endfor

by P_3. The computations are continued in this fashion until an approximation of $\hat{u}$ has been determined in $W_\ell = \mathbb{R}^n$.

In the algorithm $\Delta u_{i,m_i} := \mathrm{IM}(A_i, b_i^\delta - A_i u_{i,0})$ denotes the computation of the approximate solution $\Delta u_{i,m_i}$ of $A_i z_i = b_i^\delta - A_i u_{i,0}$ by m_i iterations with one of the iterative methods MR-II or LSQR, using the initial iterate $\Delta u_{i,0} = 0$.

The number of iterations on each level is based on the discrepancy principle as follows: we assume that there are constants c_i independent of δ, such that

$$\|b_i^\delta - \hat{b}_i\| \leq c_i \delta, \qquad 1 \leq i \leq \ell,$$

where δ satisfies (10). It can be seen by using the noise-reducing property of the restriction operators $R_i^{(\omega)}$, that a suitable choice is

$$c_i = \frac{1}{3} c_{i+1}, \qquad 1 \leq i < \ell, \qquad c_\ell = \gamma, \tag{13}$$

for some constant $\gamma > 1$. In the computed examples of Section 4, we use $\gamma = 1.4$. The discrepancy principle prescribes that the iterations on level i be terminated as soon as

$$\|b_i - A_i u_{i,0} - A_i \Delta u_{i,m_i}\| \leq c_i \delta. \tag{14}$$

When many iterations are carried out, the computed approximate solution $\Delta u_{i,m_i}$ obtained, generally, is severely contaminated by noise, which is propagated from $b_i - A_i u_{i,0}$. The purpose of the stopping criterion (14) is to i) allow enough iterations be carried out to determine an as accurate restoration on level i as possible, and ii) avoid to carry out so many iterations that the computed approximate solution $\Delta u_{i,m_i}$ is severely contaminated by propagated noise. Discussions on properties of the stopping rule (14) can be found in [8, 10]. A general discussion on applications of the discrepancy principle to determine approximate solutions of ill-posed problems is provided in [3].

The nonlinear edge-preserving prolongation operators P_i have previously been applied in [8], where further details on their implementation are provided; see also [16]. The prolongation operator P_i first maps the approximate solution

determined by the algorithm on level W_{i-1} into W_i by piecewise linear interpolation, and then uses the result as initial function for a discretized initial-boundary value problem for the Perona-Malik nonlinear diffusion equation

$$\frac{\partial u}{\partial t} = \mathrm{div}(g(|\nabla u|^2)\nabla u), \tag{15}$$

where g is the Perona-Malik diffusivity (6). Integration over a short time-interval removes noise while preserving rapid spatial transitions, such as edges. Integration is performed by carrying out about 10 time-steps of size about 0.2 with an explicit finite difference method. The small number of time-steps avoids difficulties due to numerical instability and keeps the computational work required for integration negligible. We found it to be beneficial to apply more time-steps the more noise-contaminated the available image. However, in our experience the exact choices of the number of time-steps and their sizes are not crucial for the good performance of the multilevel method.

In the algorithm, ϕ_0 denotes the initial contour for the GAC segmentation method implemented by the solving (8); see [7]. The prolongation of the level set function from W_{i-1} to W_i is carried out by spline interpolation and denoted by S_i. The statement $\phi_i := GAC(\phi_{i,0}, u_i)$ updates the contour on level i.

Ringing in restored images stems from the Gibbs phenomenon at discontinuities. The latter could be image borders, boundaries inside the image, or be introduced by inadequate spatial sampling of the image or kernel. The larger the support of the kernel in (1), the more pronounced the ringing. High contrast edges cause strong ringing, and the magnitude of the ringing is proportional to the norm of the image gradient. Based on these observations, we propose a deringing correction obtained by multiplying the image by the spatially variant function

$$\beta(x, y) = \alpha + (1 - \alpha)(1 - g(|\nabla u_{i,0}(x, y)|^2)), \tag{16}$$

where g is the diffusivity (6) and the parameter $0 \leq \alpha \leq 1$ controls the suppression of the computed correction. Since we would like to suppress ringing in the smooth regions, but avoid suppression of edges, the correction function β should be small in smooth regions and large elsewhere. We use $\alpha = 0.05$ in the computed examples of this paper, but this value can be tuned depending on the presence of large homogeneous regions in the image.

4 Numerical results

We illustrate the performance of Algorithm 1. The computations are carried out in MATLAB with about 16 significant decimal digits. We assume that a fairly accurate estimate of the norm of the noise is available. If this is not the case, such an estimate can be computed by integration of b^δ for a few time-steps with the Perona-Malik differential equation; details are described in a forthcoming paper. Note that the matrices A_i, defined by (11), do not have to be explicitly stored; it suffices to define functions for the evaluation of matrix-vector products

with the A_i and, if A_i is nonsymmetric, also with the A_i^T. For the examples of this section, the matrix-vector products can be computed efficiently by using the structure of the A_i; see, e.g., [9] for a discussion. The matrices corresponding to the finest level are numerically singular in all examples.

The displayed restored images provide a qualitative comparison of the performance of the proposed cascadic multilevel method. A quantitative comparison is given by the Peak Signal-to-Noise Ratio,

$$\mathrm{PSNR}(u_\ell, \hat{u}) = 20 \log_{10} \frac{255}{\|u_\ell - \hat{u}\|} \,\mathrm{dB}, \tag{17}$$

where $\hat{u}$ denotes the blur- and noise-free image and u_ℓ the restored image determined by Algorithm 1. Each pixel is stored with 8 bits; the numerator 255 is the largest pixel-value that can be represented with 8 bits. A high PSNR-value indicates that the restoration is accurate; however, the PSNR-values are not always in agreement with visual perception. We also measure the variation in the error image $u_{err} = u_\ell - \hat{u}$, defined by

$$\mathrm{EV}(u_\ell, \hat{u}) = \sum_{pixel} \|\nabla u_{err}\|_2^2, \tag{18}$$

where the sum is over all pixels of the image. The more accurately the edges are restored, the smaller this sum.

Fig. 1. Blur- and noise-free images used in the numerical experiments. Left: `butterfly`, 400×400 pixels. Right: `corner`, 512×512 pixels.

We apply Algorithm 1 to blur- and noise-contaminated versions of the images shown in Figure 1. The `corner` image is representative of images with well-defined edges, while the `butterfly` image is a gray-scale photographic image with smoothed edges.

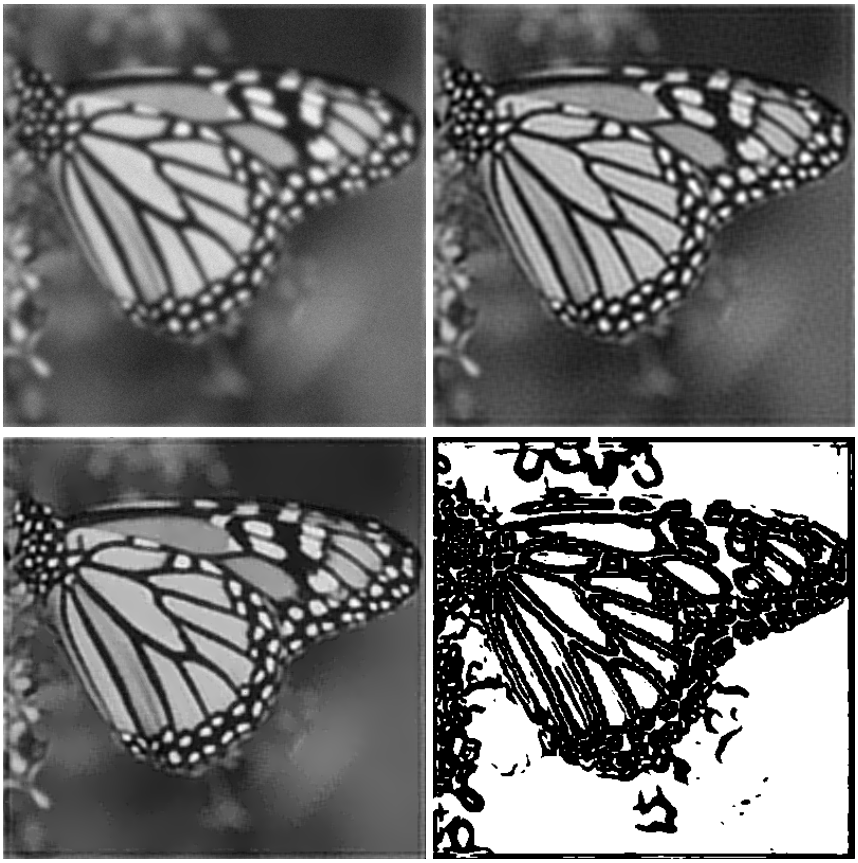

Fig. 2. Example 1. Top-left: Image contaminated by Gaussian blur and 5% Gaussian noise. Top-right: Image restored by 1-level method. Bottom-left: Image restored by 3-level method. Bottom-right: Deringing function β defined by (16).

Example 4.1. We consider the restoration of a contaminated version of the left-hand side image of Figure 1. Contamination is by space-invariant Gaussian blur as generated by the MATLAB function blur.m from Regularization Tools [6] with parameters `sigma` = 3 and `band` = 9. This function generates a block Toeplitz matrix with Toeplitz blocks. The parameter `band` specifies the half-bandwidth of the Toeplitz blocks and the parameter `sigma` defines the variance of the Gaussian PSF. The image also is contaminated by 5% Gaussian noise. The blurring operator is symmetric. We therefore use the MR-II iterative method.

Figure 2 provides a qualitative comparison of images restored by the basic 1-level MR-II method and the 3-level method defined by Algorithm 1. The restoration obtained with the latter method can be seen to be of higher quality

with sharper edges. The deringing function β (16) is shown in Figure 2 (bottom right); it is small in smooth image regions and large elsewhere.

Table 1(a) gives a quantitative comparison of the restorations determined by Algorithm 1 with $\ell = 2$ and $\ell = 3$ levels, and the basic 1-level MR-II method, for different amounts of noise. The columns marked "PSNR" and "EV" display (17) and (18), respectively. They show Algorithm 1 with $\ell = 3$ to yield images with the highest PSNR- and smallest EV-values. The column marked "iter" shows the number of iterations required on each level. For instance, the triplet $4-1-2$ indicates that Algorithm 1 carried out 4 MR-II iterations on the coarsest level, 1 iteration on the intermediate level, and 2 iterations on the finest level. The dominating computational effort are the matrix-vector product evaluations on the finest level. The 2- and 3-level methods can be seen to require fewer iterations on the finest level than the basic 1-level MR-II method. □

ℓ	% noise	PSNR	iter	EV
1	1	26.05	11	5043
2	1	26.73	8 9	4179
3	1	26.86	9 7 9	4060
1	5	24.30	4	5279
2	5	24.38	3 3	4682
3	5	24.63	5 3 3	4555
1	10	23.25	3	5477
2	10	23.42	2 2	4949
3	10	23.60	4 1 2	4853

(a)

ℓ	% noise	PSNR	iter	EV
1	1	30.93	12	4629
2	1	31.69	11 9	2294
3	1	32.02	17 8 8	2251
1	5	27.13	5	6519
2	5	28.56	4 3	3553
3	5	28.69	7 2 3	3140
1	10	25.15	3	5368
2	10	26.77	2 2	3692
3	10	26.93	3 1 2	3466

(b)

Table 1. PSNR, number of iterations (iter), and edge variation (EV) as functions of the number of levels ℓ and noise-level ν for restorations of (a) the image of Example 4.1 contaminated by Gaussian blur determined by `band` $= 9$ and `sigma` $= 3$, and (b) the image of Example 4.2 contaminated by motion blur defined by $r = 15$ and $\theta = 10$.

Example 4.2. Consider the restoration of a version of the right-hand side image of Figure 1 that has been contaminated by motion blur and 5% Gaussian noise. The PSF is represented by a line segment of length r pixels in the direction of the motion. The angle θ (in degrees) specifies the direction; it is measured counter-clockwise from the positive x-axis. The PSF takes on the value r^{-1} on this segment and vanishes elsewhere. We refer to the parameter r as the width. The motion blur for this example is defined by $r = 15$ and $\theta = 10$. The blurring matrix A is nonsymmetric. We therefore use the LSQR iterative method in Algorithm 1.

Figure 3 (left) shows the restoration determined by Algorithm 1 with 3 levels. The restored image obtained by the basic 1-level LSQR method is shown in Figure 3 (right). Visual comparison shows Algorithm 1 to give the most pleasing restoration. This is in agreement with the PSNR- and EV-values reported in Table 1(b). □

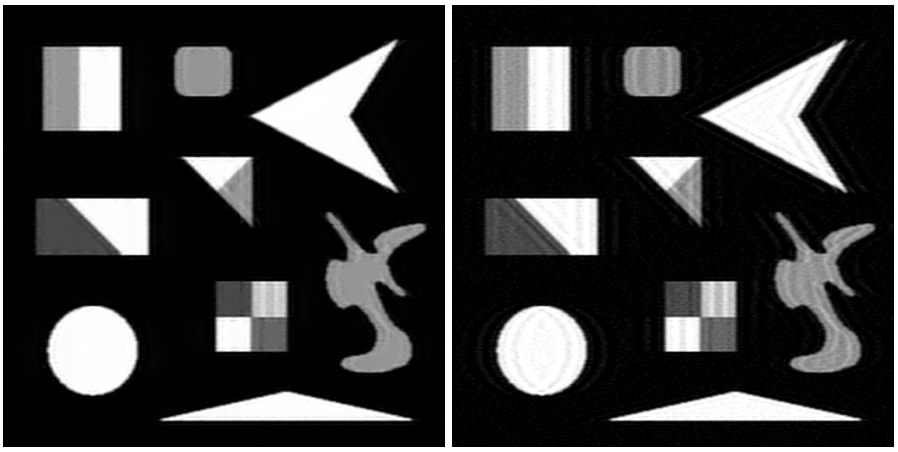

Fig. 3. Example 4.2. Left: Restoration determined by 3-level LSQR-based multilevel method. Right: Restoration obtained by basic 1-level LSQR.

Example 4.3. We apply Algorithm 1 to segmentation of a contaminated version of the image of Figure 1 (left). The contamination is caused by Gaussian blur, determined by `band` = 9 and `sigma` = 3, and 10% Gaussian noise. Segmentation is carried out using the variational formulation for geodesic active contours (GAC) without re-initialization as described by Li et al. [7]. The initial curve is close to the boundary of the image. Figure 4 (top-left) shows the segmentation obtained when applied to the noise- and blur-free image in Figure 1 (left). The curve evolution requires 900 iterations.

Segmentation of the contaminated image is more difficult. We first deblur the contaminated image by the basic 1-level MR-II iterative method, and then apply GAC segmentation to the restored image. The resulting segmentation is shown in Figure 4 (top-right). The curve evolution required 1200 iterations.

Finally, we apply Algorithm 1 with 3 levels and the Segmentation step. No segmentation is carried out on the coarsest level. On level $\ell = 2$, we apply GAC segmentation with 400 curve evolution iterations. The resulting segmentation is shown in Figure 4 (bottom-left). Prolongation of the evolved contour is carried out by spline interpolation. Only 100 curve evolution iterations are required on the finest level. The resulting segmentation is displayed in Figure 4 (bottom-right). The figure shows Algorithm 1 to be able to extract object boundaries with less computational effort and higher accuracy than the corresponding 1-level method. □

5 Conclusions and extension

Visual inspection of the images shown in Section 4, as well as computed PSNR- and EV-values, show the cascadic multilevel method to give more accurate

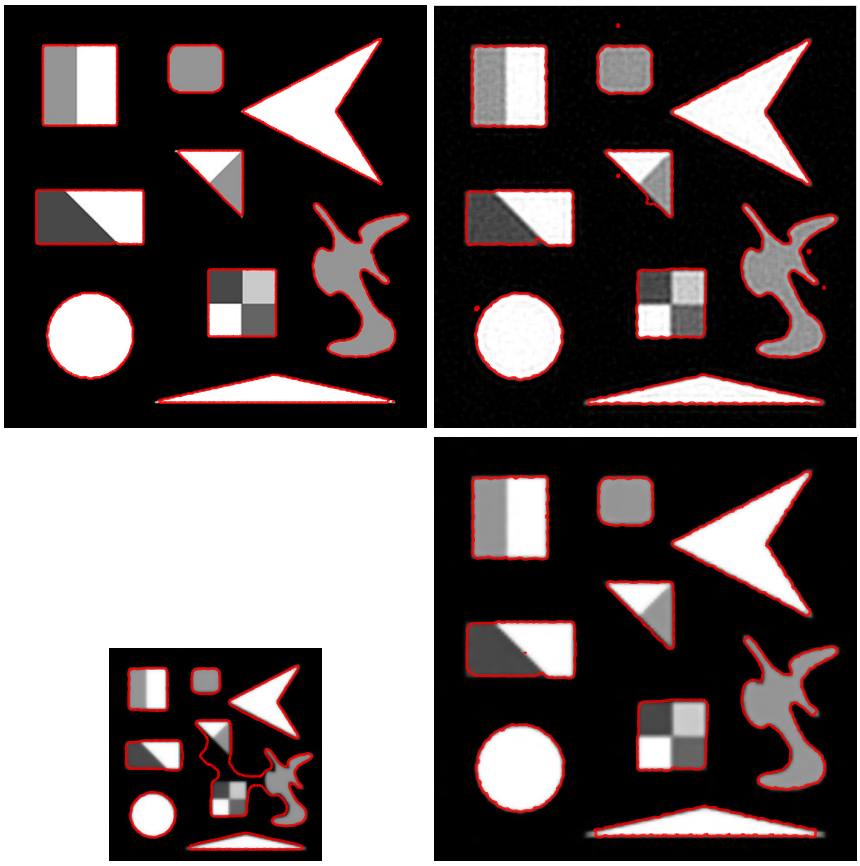

Fig. 4. Example 3. Top left: Segmentation of a blur- and noise- free image. Top right: Segmentation a blurred and noisy image by a 1-level method. Bottom-left: Segmentation by 3-level method of the blurred and noisy image on level 2. Bottom-right: Segmentation by 3-level method on finest level.

restorations than 1-level methods applied on the finest level only. A multilevel approach to segmentation of contaminated images also yields better results and requires less computational effort than the corresponding 1-level method. The aim of ongoing work is to gain increased understanding of the interplay between image restoration and segmentation.

Acknowledgments

This research has been supported by PRIN-MIUR-Cofin 2006 project, by University of Bologna "Funds for selected research topics", and in part by an OBR Research Challenge Grant.

References

1. A. Buades, B. Coll, and J. M. Morel, The staircasing effect in neighborhood filters and its solution, IEEE Trans. Image Processing 15, 1499–1505 (2006).
2. V. Caselles, R. Kimmel, and G. Sapiro, Geodesic active contours, Int. J. Comput. Vis. 22 , 61–79 (1997).
3. H. W. Engl, M. Hanke, and A. Neubauer, Regularization of Inverse Problems, Kluwer, Dordrecht, 1996.
4. M. Hanke, Conjugate Gradient Type Methods for Ill-Posed Problems, Longman, Essex, 1995.
5. P. C. Hansen, *Rank-Deficient and Discrete Ill-Posed Problems*, SIAM, Philadelphia, 1997.
6. P. C. Hansen, Regularization tools, version 4.0 for MATLAB 7.3, Numer. Algorithms 46, 189–294 (2007).
7. C. Li, C. Xu, C. Gui, and M. D. Fox, Level set evolution without re-initialization: a new variational formulation, Proc. IEEE Conf. Computer Vision and Pattern Recognition 1, IEEE Computer Soc., 430–436 (2005).
8. S. Morigi, L. Reichel, F. Sgallari, and A. Shyshkov, Cascadic multiresolution methods for image deblurring, SIAM J. Imaging Sci. 1, 51–74 (2008).
9. M. K. Ng, R. H. Chan, and W.-C. Tang, A fast algorithm for deblurring models with Neumann boundary conditions, SIAM J. Sci. Comput. 21 , 851–866 (1999).
10. L. Reichel and A. Shyshkov, Cascadic multilevel methods for ill-posed problems, J. Comput. Appl. Math., in press
11. L. Rudin, S. Osher, and E. Fatemi, Nonlinear total variation based noise removal algorithms, Physica D 60, 259–268 (1992).
12. S. Osher and J. A. Sethian, Fronts propagating with curvaturedependent speed: algorithms based on Hamilton-Jacobi formulations, J. Comput. Phys. 79, 12–49 (1988).
13. C. C. Paige and M. A. Saunders, LSQR: An algorithm for sparse linear equations and sparse least squares, ACM Trans. Math. Software 8 ,43–71 (1982).
14. P. Perona and J. Malik, Scale-space and edge detection using anisotropic diffusion, IEEE Trans. Pattern Anal. Mach. Intell. 12, 629–639 (1990).
15. M. Welk, D. Theis, T. Brox, and J. Weickert, PDE-based deconvolution with forward-backward diffusivities and diffusion tensors. In R. Kimmel, N. Sochen, and J. Weickert (Eds.): Scale-Space and PDE Methods in Computer Vision, Lecture Notes in Computer Science, vol. 3459, Springer, Berlin, 585–597 (2005).
16. J. Weickert, B. M. H. Romeny, and M. A. Viergever, Efficient and reliable schemes for nonlinear diffusion filtering, IEEE Trans. Image Process. 7, 398–410 (1998).